



HAL
open science

Visualizing gas evolution on graphite and oxygen-evolving anodes

Laurent Cassayre, Torstein A. Utigard, Sylvie Bouvet

► **To cite this version:**

Laurent Cassayre, Torstein A. Utigard, Sylvie Bouvet. Visualizing gas evolution on graphite and oxygen-evolving anodes. *JOM Journal of the Minerals, Metals and Materials Society*, 2002, 54 (5), pp.41-45. 10.1007/BF02701696 . hal-02400252

HAL Id: hal-02400252

<https://hal.science/hal-02400252>

Submitted on 9 Dec 2019

HAL is a multi-disciplinary open access archive for the deposit and dissemination of scientific research documents, whether they are published or not. The documents may come from teaching and research institutions in France or abroad, or from public or private research centers.

L'archive ouverte pluridisciplinaire **HAL**, est destinée au dépôt et à la diffusion de documents scientifiques de niveau recherche, publiés ou non, émanant des établissements d'enseignement et de recherche français ou étrangers, des laboratoires publics ou privés.




Open Archive Toulouse Archive Ouverte (OATAO)

OATAO is an open access repository that collects the work of Toulouse researchers and makes it freely available over the web where possible

This is an author's version published in: <http://oatao.univ-toulouse.fr/25124>

Official URL: <https://doi.org/10.1007/BF02701696>

To cite this version:

Cassayre, Laurent  and Utigard, Torstein A. and Bouvet, Sylvie *Visualizing gas evolution on graphite and oxygen-evolving anodes*. (2002) JOM Journal of the Minerals, Metals and Materials Society, 54 (5). 41-45. ISSN 1047-4838

Any correspondence concerning this service should be sent to the repository administrator: tech-oatao@listes-diff.inp-toulouse.fr

Visualizing Gas Evolution on Graphite and Oxygen-Evolving Anodes

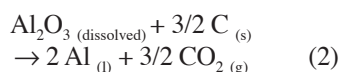
Laurent Cassayre, Torstein A. Utigard, and Sylvie Bouvet

Recent progress in material science might soon allow the replacement of the consumable carbon anode by an inert material. This is likely to induce changes in the overall process, and particularly in the gas evolution. Video recordings of oxygen-evolving anodes (SnO_2 , Cu, Cu-Ni) and carbon anodes were performed in laboratory electrolysis cells, using direct observation from above, a see-through cell, and radiography techniques. The gas behavior was very different between the two kinds of anodes, and probably linked to the wettability of the material by the electrolyte.

INTRODUCTION

Replacement of carbon anodes by non-consumable (or inert) materials has been a subject of research since the invention of the Hall-Héroult process more than a hundred years ago. With the proper material, inert anodes would offer potential savings in operating costs by eliminating carbon anode replacement and by providing tighter control of the anode-cathode distance. As presented by the following equations, the use of an oxygen-evolving anode

(Equation 1) could also help suppress the emissions of greenhouse gases, which are a growing concern with the current process (Equation 2).



While a vast array of materials has already been patented for inert-anode application, none is yet in commercial use. This is mainly because the severe operating environment and the need for good electronic conductivity limits the number of suitable materials. Most recent research has concentrated on metals, oxide ceramics, and cermets.¹ In the present study, copper, copper-nickel alloy (wt.% 75/25), and tin-oxide materials were tested as oxygen-evolving anodes, even if none of them is stable enough to totally resist corrosion.

Modifying the anodic material is likely to induce many changes in the overall process; cell voltage, bath resistivity, and gas evolution are, indeed, deeply linked with anode properties. The aim of the current work was to

compare the gas behavior between oxygen-evolving and graphite anodes, and to characterize the bubble size and the bubble-layer depth in the inter-electrode area. Video recordings of electrolysis at various current densities (CD) were performed in laboratory cells, using direct observation from above and see-through-cell²⁻⁴ and radiography^{5,6} techniques. The influence of the alumina content in the electrolyte was studied for graphite and tin oxide. A comparison of the wettability of the materials by the electrolyte was also carried out to try to explain the very different gas behavior observed.

EXPERIMENTAL SETTINGS

Three different methods were used to get video recordings of the gas evolution at the anode during alumina electrolysis. Schematics of the experimental techniques are presented in Figure 1.

Direct observations from above the bath were carried out in a small furnace open to the air with a microscope positioned above the cell. The cathode was a graphite cylinder ($\varnothing = 5$ mm), while the anode was a graphite or tin-oxide cylinder ($\varnothing = 5$ mm).

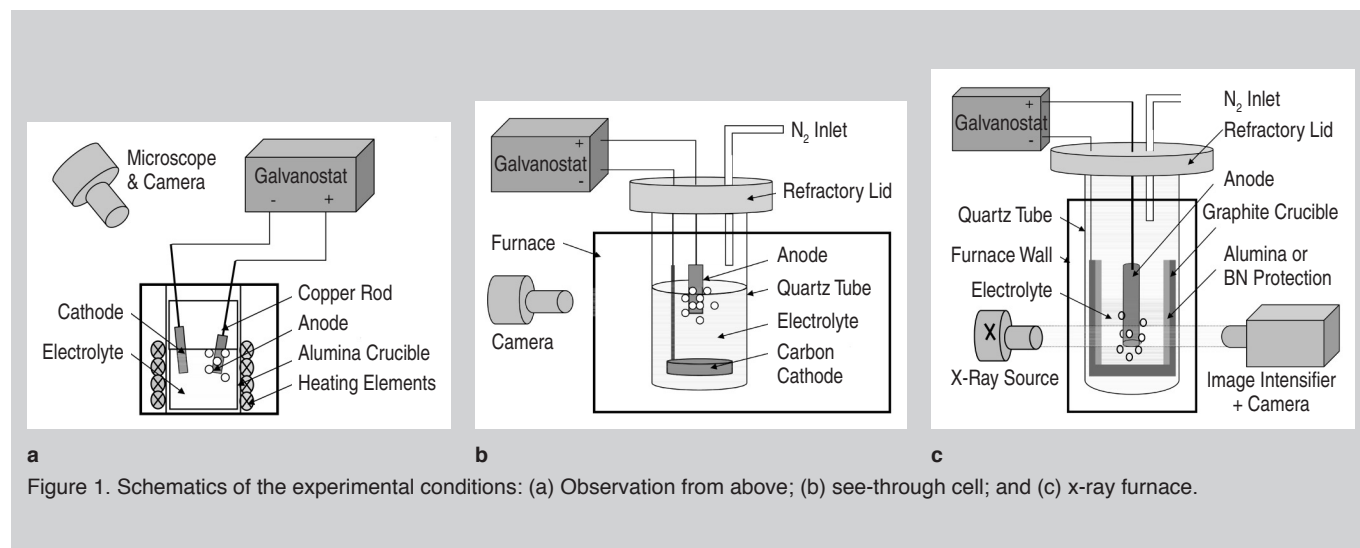


Figure 1. Schematics of the experimental conditions: (a) Observation from above; (b) see-through cell; and (c) x-ray furnace.

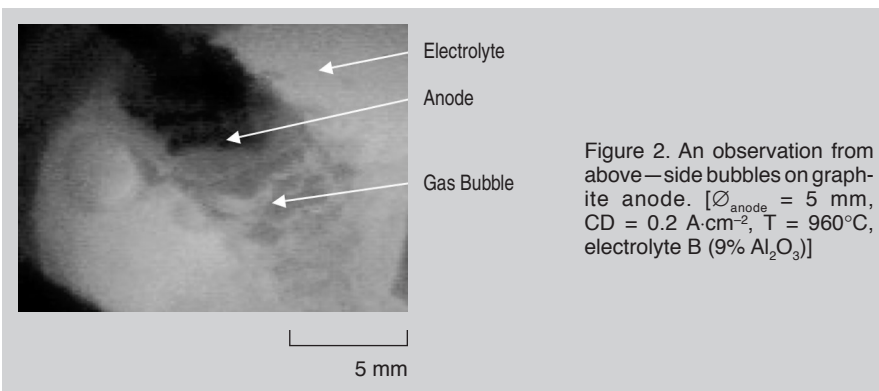


Figure 2. An observation from above—side bubbles on graphite anode. [$\varnothing_{\text{anode}} = 5 \text{ mm}$, $\text{CD} = 0.2 \text{ A}\cdot\text{cm}^{-2}$, $T = 960^\circ\text{C}$, electrolyte B (9% Al_2O_3)]

Electrolysis was also carried out in transparent quartz tubes ($\varnothing_{\text{in}} = 54 \text{ mm}$) placed in an electric furnace, allowing lateral observations through a hole in the front panel. In this see-through cell,

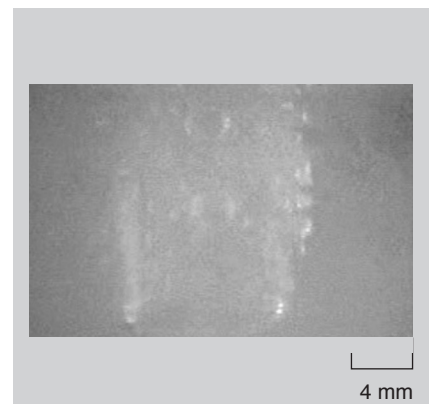


Figure 3. A graphite anode during electrolysis in see-through cell. [$\varnothing_{\text{anode}} = 9 \text{ mm}$, $\text{CD} = 0.2 \text{ A}\cdot\text{cm}^{-2}$, $T = 960^\circ\text{C}$, electrolyte B (9% Al_2O_3), $\text{ACD} = 2 \text{ cm}$]

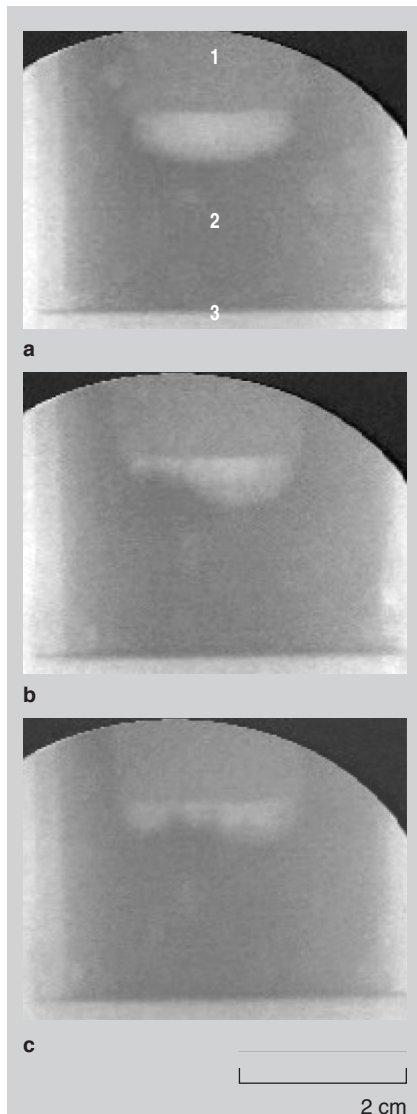


Figure 4. A graphite anode during electrolysis in x-ray furnace; (a) $\text{CD} = 0.4 \text{ A}\cdot\text{cm}^{-2}$, 1 = electrode, 2 = electrolyte, and 3 = graphite crucible; (b) $\text{CD} = 1 \text{ A}\cdot\text{cm}^{-2}$; and (c) $\text{CD} = 1.6 \text{ A}\cdot\text{cm}^{-2}$. [$\varnothing_{\text{anode}} = 18 \text{ mm}$, $T = 960^\circ\text{C}$, electrolyte A (2.5% Al_2O_3), $\text{ACD} = 2 \text{ cm}$]

the cathode was a graphite cylinder ($\varnothing = 43 \text{ mm}$, $h = 15 \text{ mm}$) located at the bottom of the tube, and the anode was either a graphite or tin-oxide cylinder ($\varnothing = 9 \text{ mm}$, $h = 50 \text{ mm}$), vertically positioned 2 cm above the cathode. A new quartz tube was used for each experiment.

Radiography tests consisted of performing electrolysis in a graphite crucible ($\varnothing_{\text{in}} = 45 \text{ mm}$) placed in a vertical quartz tube and heated in a di-moly silicide resistor furnace. Images of the anode immersed in the electrolyte were obtained from an x-ray beam passing through whole system. An electrically insulating alumina cylinder protected the inside walls of the crucible from the electrolyte so that current distribution was kept vertical through the bath. A boron-nitride cylinder was used for the same purpose with low alumina-content electrolytes. Anodes ($\varnothing = 18 \text{ mm}$, $h = 50 \text{ mm}$) were made of ATJ graphite, tin oxide, pure copper, or copper-nickel alloy (wt.% 75/25). The atmosphere in the cell was purged with nitrogen before heating, and a small flow was kept during the runs to prevent carbon oxidation.

Two different electrolyte compositions were used, based on a mix of cryolite with AlF_3 (11 wt.%), Al_2O_3 , and CaF_2 (5 wt.%). Weight fraction of alumina was either 2.5 wt.% (electrolyte A) or 9 wt.% (electrolyte B), electrolyte B being saturated in alumina.⁷ The mix of powders was pre-melted at $1,000^\circ\text{C}$ in graphite crucibles, then cast, crushed, and stored in a dessicator.

BUBBLING AT THE GRAPHITE ANODE

Bubble formation on the side of a graphite anode was observed from above at small CDs (0.05 to $0.2 \text{ A}\cdot\text{cm}^{-2}$). Bubble birth occurs on specific nucleation

spots, at a frequency growing with CD. Increasing CD leads also to a large number of nucleation sites. Round-shaped bubbles grow and coalesce until reaching 2–3 mm in diameter, then detach and escape vertically. As shown in Figure 2, the surface coverage of the anode is very high. The bubbles are stuck on the anode and, without much agitation in the bath, detach with difficulty.

Tests in see-through cells were limited in time (no more than 7 minutes) and CD (up to $0.5 \text{ A}\cdot\text{cm}^{-2}$), because streamers rapidly arose in the cell and lead to an opaque electrolyte. This fog was attributed to dissolved aluminum produced at the cathode,^{2,4} and did not fade as reported by some authors.⁸ Observations at industrial CDs (around $0.7 \text{ A}\cdot\text{cm}^{-2}$) could not be performed, diminishing the interest of the method.

Video recordings of gas evolution during both see-through-cell and radiographic experiments confirmed previous observations described in the literature:^{3,9} a periodic gas mechanism release occurs at the bottom of the anode, leading to important variations with time in the amount of gas trapped in the inter-electrode area. At small CDs (up to around $0.5 \text{ A}\cdot\text{cm}^{-2}$), several bubbles form on the bottom surface of the anode, then grow and coalesce until a single large bubble covers the whole area and is finally released, leaving a clean surface free of gas. Figure 3 shows the bubble trapped under the anode, just before release, during see-through cell electrolysis at $0.2 \text{ A}\cdot\text{cm}^{-2}$.

At higher CDs (studied only by

x-ray experiments), coalescence does not happen as much as at low CDs, and bubbles escape before covering the whole anode, as illustrated in Figure 4. The average bubble diameter before release, calculated as the mean diameter of ten bubbles for each CD, is presented in Figure 5. The diameter decreases from around 18 mm at $0.2 \text{ A}\cdot\text{cm}^{-2}$ to 7 mm at $1.6 \text{ A}\cdot\text{cm}^{-2}$. The alumina content in the electrolyte does not have a major influence on the bubble size.

The release frequency of the CO_2 bubbles is also strongly related to the current density, as shown in Figure 6. These values agree with those obtained on 10 cm diameter anodes by monitoring the fluctuations of the bath level,¹⁰ but significantly higher than those calculated by cell voltage analysis³ using 1 cm diameter anodes.

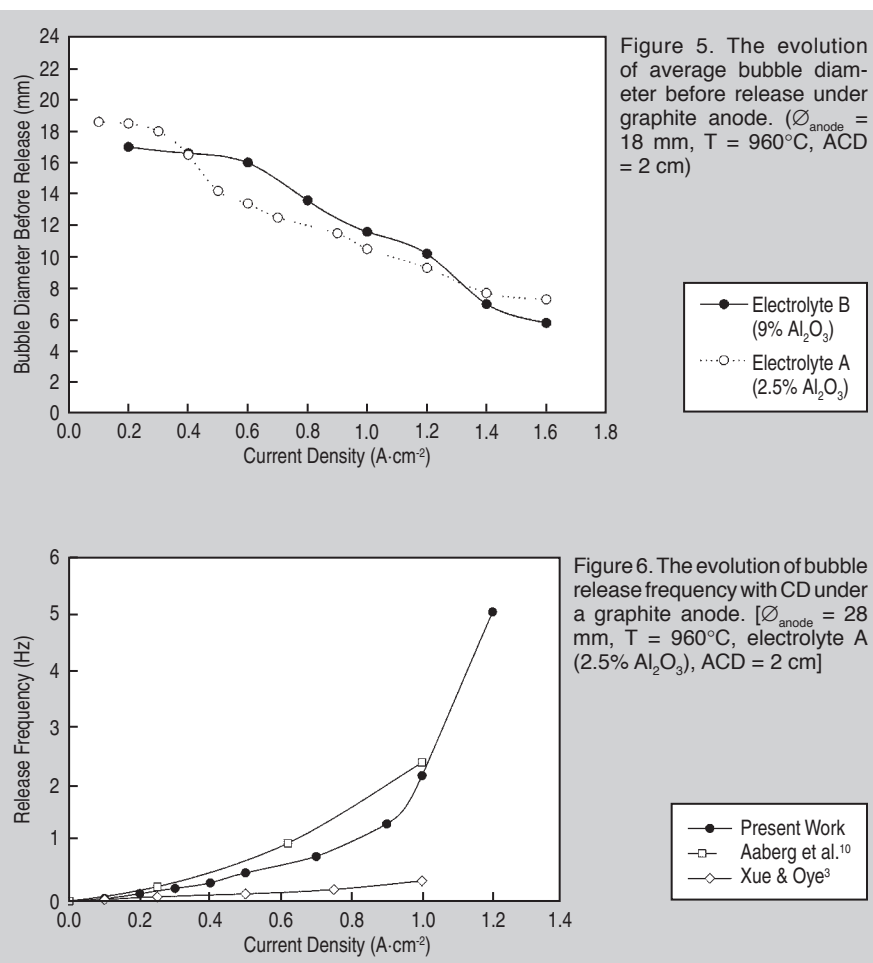
BUBBLING AT OXYGEN-EVOLVING ANODES

Gas evolution is nearly identical for tin-oxide, copper, and copper-nickel anodes, but was found to be very different as compared to what was observed on the graphite anode.

Observations of a tin-oxide anode from above showed tiny bubbles escaping continuously without much coalescence, forming a foam around the electrode, as illustrated in Figure 7. The bubble diameter, measured under the microscope (40 x), was estimated to be around 0.1 mm, which is ten to 30 times smaller than on graphite anodes.

Some tests were run in see-through cells, but observations were difficult because the froth of bubbles hid the electrode even at low CDs ($0.1 \text{ A}\cdot\text{cm}^{-2}$). This resulted in poor contrast between the electrolyte and the gas. Furthermore, bath mist occurred very quickly, the same way as described when using graphite anodes.

Radiographic observation proved to be more adapted to the study of the gas evolution on oxygen-evolving anodes. The anode appears in black and the bath in dark grey, while gas takes the form of a light grey halo around and under the electrode (Figure 8). As almost no coalescence occurs between the tiny bubbles, gas release looks continuous and the gas foam under the electrode keeps roughly a constant shape at



fixed CD.

The depth of the gas layer under the anode is plotted as a function of CD and material in Figure 9. The evolution is almost identical for the three oxygen-evolving electrodes: the bubble layer thickness grows regularly with CD until reaching 2–2.5 mm at $1 \text{ A}\cdot\text{cm}^{-2}$. Increasing CD over $1 \text{ A}\cdot\text{cm}^{-2}$ doesn't increase the penetration of the gas under the anode, maybe because the volume fraction of the gas in the bubble layer increases. However, the contrast of the x-ray images was not sufficient to observe noticeable changes in the brightness of the gas froth, as it could be expected with a higher gas density. Another possibility is that the release velocity of the bubbles increases, leading to a shorter residence time of the bubbles under the anode.

When testing electrolyte A (2.5% Al_2O_3) on a tin-oxide anode, no difference was seen in the gas behavior as compared to the electrolyte B (9% Al_2O_3).

Figure 9 shows that the bubble layer under the graphite anode is decreasing with CD, from 5 mm to 4.2 mm, confirming both the values and the

trend reported by Aaberg et al.¹⁰ At $1 \text{ A}\cdot\text{cm}^{-2}$, gas penetration under the anode is roughly twice as deep with graphite than with oxygen-evolving anodes, which is important with regards to the setting of the anode-cathode distance.

WETTING OF THE ANODES

The angle of contact, θ , is a measure of the degree of wetting of a solid

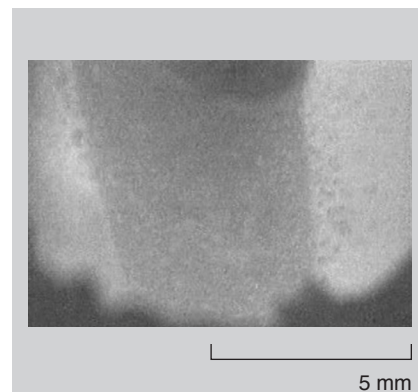


Figure 7. An observation from above-side bubbles on tin-oxide anode. [$\varnothing_{\text{anode}} = 5 \text{ mm}$, $\text{CD} = 0.2 \text{ A}\cdot\text{cm}^{-2}$, $T = 960^\circ\text{C}$, electrolyte B (9% Al_2O_3), $\text{ACD} = 2 \text{ cm}$]

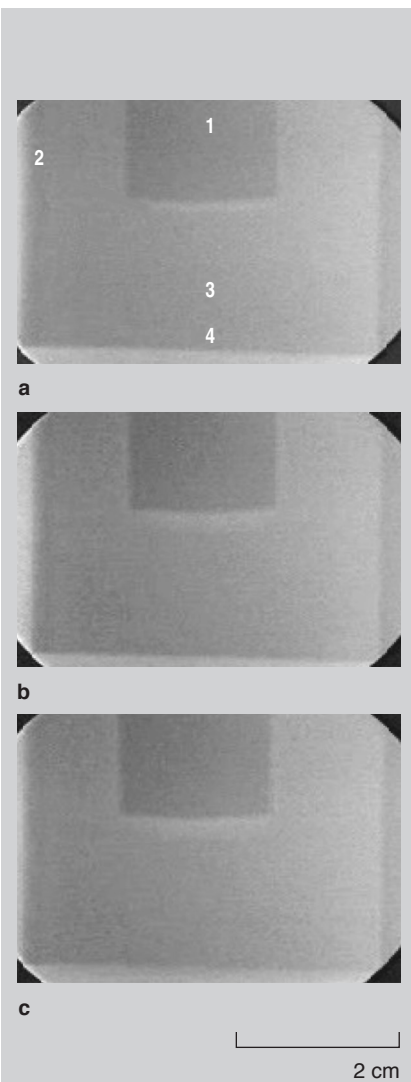


Figure 8. A tin-oxide anode during electrolysis in x-ray furnace. (a) $CD = 0.2 \text{ A}\cdot\text{cm}^{-2}$, 1 = anode, 2 = gas layer, 3 = electrolyte, and 4 = graphite crucible; (b) $CD = 1 \text{ A}\cdot\text{cm}^{-2}$; and (c) $CD = 1.6 \text{ A}\cdot\text{cm}^{-2}$ [$\varnothing_{\text{anode}} = 18 \text{ mm}$, $T = 960^\circ\text{C}$, electrolyte B ($9\% \text{ Al}_2\text{O}_3$), $ACD = 2 \text{ cm}$]

surface by a liquid phase. In the case of regular aluminum electrolysis, θ is dependant on the composition of the melt, the physical properties of the carbon material, the temperature, the composition of the gaseous phase, and the current density.¹¹ An interesting point is that, as suggested by Vogt,¹² a decrease of this contact angle might be correlated to an increased bubble size. It was then decided to use a hot-stage microscope to study the wetting of graphite, tin-oxide, copper, and copper-nickel alloy by the electrolyte, in order to explain the difference in bubble size observed during electrolysis.

Thirty-five milligrams of electrolyte B

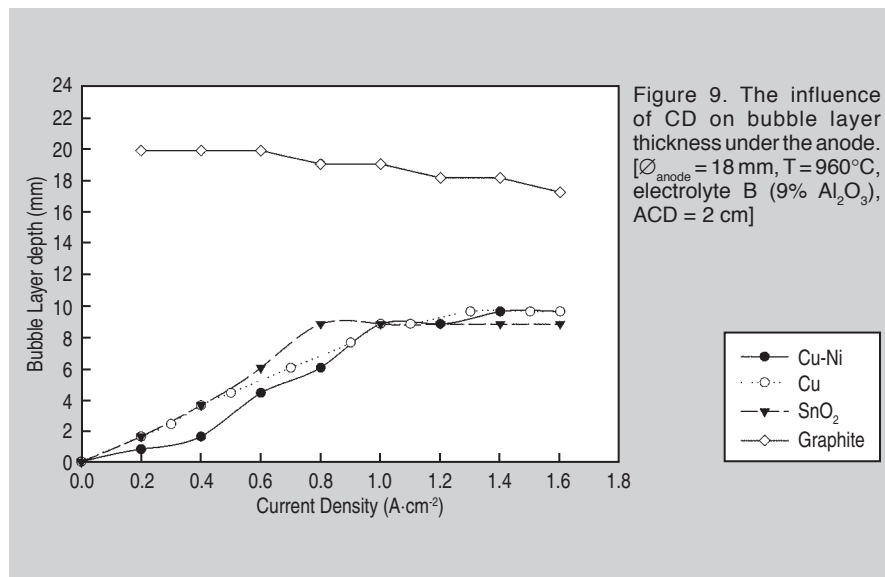


Figure 9. The influence of CD on bubble layer thickness under the anode. [$\varnothing_{\text{anode}} = 18 \text{ mm}$, $T = 960^\circ\text{C}$, electrolyte B ($9\% \text{ Al}_2\text{O}_3$), $ACD = 2 \text{ cm}$]

($9\% \text{ Al}_2\text{O}_3$) were placed on a horizontal solid sample ($\varnothing = 10 \text{ mm}$) and quickly heated to around $1,000^\circ\text{C}$. A video camera mounted on a microscope recorded the melting of the bath on the sample. Experiments were usually carried out in the air, except for some tests on graphite samples performed in CO_2 .

The contact angle of molten electrolyte on a graphite sample was measured around $120\text{--}130^\circ$, which is consistent with literature values.¹¹ The influence of the gaseous phase (air or CO_2) on the wettability could not be determined; it was not significant compared to the measurement uncertainties of the contact angle ($\pm 5^\circ$). Graphite is thus poorly wetted by the electrolyte, as illustrated in Figure 10.

Wetting on tin oxide was found to be very different. As shown in Figure 11, the electrolyte started to spread as soon as it began to melt, and then rapidly covered the top surface and the sides of the sample. Contact angle is therefore close to zero. Copper and copper-nickel samples were also very well wetted by the electrolyte.

According to the preceding results,

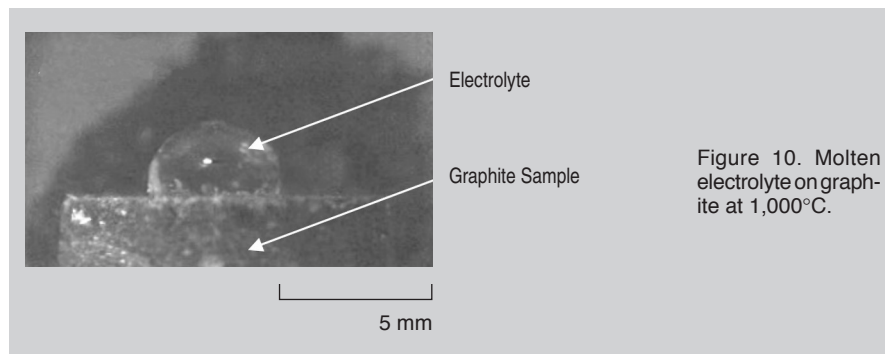


Figure 10. Molten electrolyte on graphite at $1,000^\circ\text{C}$.

the size of the bubbles released during alumina electrolysis could be related to the wettability of the anode by the electrolyte. The bubbles formed on tin oxide, copper, and copper-nickel, all very well wetted by the electrolyte, will detach easily from their nucleation site, while bubbles formed on carbon are stuck and grow before detachment.

CONCLUSIONS

The characterization of the bubble layer under the anode, summarized in Table I, showed many differences between the two types of anodes, which could have important consequences in the overall process:

- Given that the bubble layer is thin and keeps a constant shape on oxygen-evolving anodes, a smaller anode-cathode distance than currently used on carbon anodes could be set and help save energy by reducing the ohmic losses through the bath.
- Bath stirring, which is necessary to keep a constant alumina concentration close to the electrodes, might be significantly reduced.

References

1. R.P.Pawlek, "Inert Anodes for the Primary Aluminium Industry: An Update," *Light Metals 1996*, ed. W. Hale (Warrendale, PA: TMS, 1996), p. 243.
2. W.E. Haupin, "See-through Hall-Héroult Cell," *Aluminium*, 4 (1975), p. 273.
3. J. Xue and H. Øye, "Bubble Behaviour—Cell Voltage Oscillation during Aluminium Electrolysis and the Effects of Sound and Ultrasound," *Light Metals 1995*, ed. J. Evans (Warrendale, PA: TMS, 1995), p. 265.
4. Q. Zhuxian et al., "Formation of Metal Fog during Molten Salt Electrolysis Observed in See-through Cell," *J. Appl. Electrochem.*, 17 (1987), p. 707.
5. T.A. Utigard, J.M. Toguri, and S.W. Ip, "Direct Observation of the Anode Effect by Radiography," *Light Metals 1988*, ed. L.G. Boxall (Warrendale, PA: TMS, 1988), p. 703.
6. T.A. Utigard, H. Costa, and P. Popelar, "Visualization of the Hall-Héroult Process," *Light Metals 1994*, ed. U. Mannweiler (Warrendale, PA: TMS, 1994), p. 233.
7. A. Solheim et al., "Liquidus Temperature and Alumina Solubility in the System $\text{Na}_3\text{AlF}_6\text{-AlF}_3\text{-LiF-CaF}_2\text{-MgF}_2$," in Ref. 3, p. 456.
8. Q. Zhuxian, F. Liman, Shenyang, and K. Grotheim, *Aluminium*, 5 (1986), p. 341.
9. T.A. Utigard and J.M. Toguri, "Anode Gas Behaviour during Electrolysis," in Ref. 3, p. 265.
10. R.J. Aaberg et al., "The Gas under Anodes in Aluminium Smelting Cells Part II: Gas Volume and Bubble Layer Characteristics," *Light Metals 1997*, ed. R. Huglen (Warrendale, PA: TMS, 1997), p. 341.
11. K. Grjotheim et al., *Aluminium Electrolysis: Fundamentals of the Hall-Héroult Process*, 2nd edition (Dusseldorf, Germany: Aluminium Verlag, 1982), p. 146.
12. H. Vogt, "Contribution to the Interpretation of the Anode Effect," *Electrochimica Acta*, 42 (1997), p. 2695.

Laurent Cassayre is a research assistant and Tortein Utigard is a professor in the Materials Science and Engineering Department at the University of Toronto. Sylvie Bouvet is with Pechiney CRV.

For more information, contact L. Cassayre, University of Toronto, Materials Science and Engineering Department, 184 College, Room 145/WB, Toronto, Ontario, Canada M5S 3E4; e-mail laurent_cassayre@yahoo.fr.

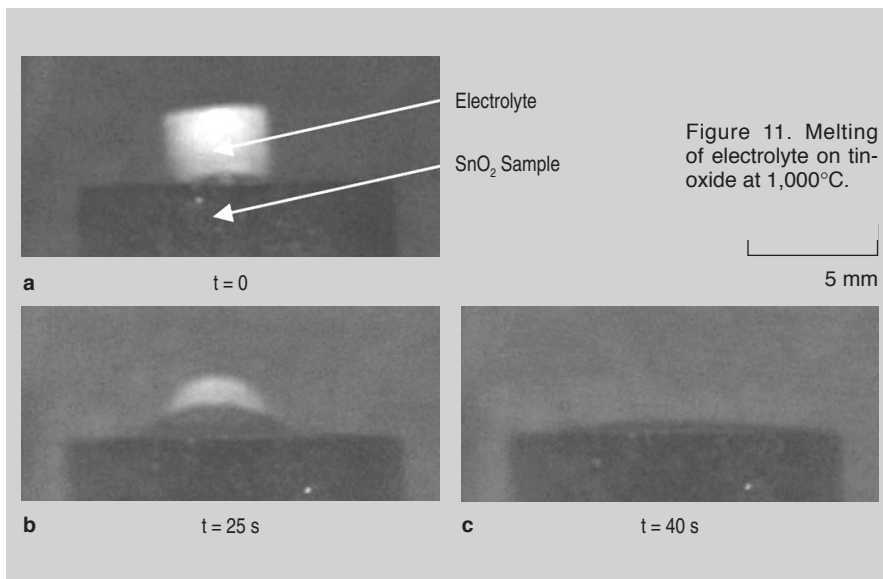


Figure 11. Melting of electrolyte on tin-oxide at 1,000°C.

Table I. Summary of the Gas Evolution

Anodic Material	Bubbling	Bubble Diameter	Bubble Layer Depth
Graphite	Periodic release of large bubbles	2–10 mm	~ 5 mm
Oxygen-evolving	Froth of tiny bubbles	0.1 mm	~ 2 mm

$\varnothing_{\text{anode}} = 18 \text{ mm}$; $\text{CD} = 1 \text{ A}\cdot\text{cm}^{-2}$; $T = 960^\circ\text{C}$; electrolyte B (9% Al_2O_3); $\text{ACD} = 2 \text{ cm}$

- The back reaction (reoxidation of the aluminum produced at the cathode and dissolved in the bath) might be favored by the increase of the gas/electrolyte area due to the small size of the bubbles.

The study of three different oxygen-evolving anodes showed that a good wetting by the electrolyte leads to the formation of tiny bubbles. Contact

angle measurements of the system electrolyte-anode-oxygen might then allow predicting the gas evolution on other candidate as inert anodes materials without having recourse to heavy equipment like the x-ray furnace.

ACKNOWLEDGEMENTS

The authors are grateful to Pechiney for the financial support of this work.